

Theory of the circular closed loop antenna in the terahertz, infrared, and optical regions

A. F. McKinley, T. P. White, and K. R. Catchpole

Citation: *J. Appl. Phys.* **114**, 044317 (2013); doi: 10.1063/1.4816619

View online: <http://dx.doi.org/10.1063/1.4816619>

View Table of Contents: <http://jap.aip.org/resource/1/JAPIAU/v114/i4>

Published by the [AIP Publishing LLC](#).

Additional information on J. Appl. Phys.

Journal Homepage: <http://jap.aip.org/>

Journal Information: http://jap.aip.org/about/about_the_journal

Top downloads: http://jap.aip.org/features/most_downloaded

Information for Authors: <http://jap.aip.org/authors>

ADVERTISEMENT



Now Indexed in
Thomson Reuters
Databases

Explore AIP's open access journal:

- Rapid publication
- Article-level metrics
- Post-publication rating and commenting

Theory of the circular closed loop antenna in the terahertz, infrared, and optical regions

A. F. McKinley,^{a)} T. P. White, and K. R. Catchpole

Centre for Sustainable Energy Systems, Research School of Engineering, The Australian National University, Canberra ACT 0200, Australia

(Received 11 May 2013; accepted 10 July 2013; published online 29 July 2013)

Modern antenna theory forms the bulwark of our knowledge of how radiation and metallic structures interact in the radio frequency (RF) and microwave (MW) regions. The theory has not yet penetrated the terahertz, infrared, and optical regions to the same degree. In this paper, we provide a rigorous analysis of closed circular loop antennas from first principles. Using antenna theory, we tie together their long wavelength behavior with their behavior at short wavelengths through the visible region. We provide analytic forms for the input impedance, current, quality factor, radiation resistance, ohmic loss, and radiation efficiency. We provide an exact circuit model for the closed loop in the RF and MW regions, and extend it through the optical region. We also provide an implicit analytic form for the determination of all modal resonances, allowing prediction of the resonance saturation wavelength for loops. Through simulations, we find that this behavior extends to hexagonal and square loops. All results are applicable to loop circumferences as short as 350 nm. Finally, we provide a precise analytic model of the index of refraction, as a tool in these computations, which works equally well for metals and semi-conductors.

© 2013 AIP Publishing LLC. [<http://dx.doi.org/10.1063/1.4816619>]

I. INTRODUCTION

For decades, studies of radio frequency (RF) and microwave (MW) antennas have produced an immense literature on the interaction between radiation and resonant metallic structures. Antenna theory at low frequencies uses classical electromagnetic theory to calculate internal current distributions, and from these, bandwidth, quality factor (Q), radiation resistance, radiation power density patterns, gain, and directivity. Primarily, the theory calculates input impedance and using it, models the antenna's resistance, inductance, and capacitance (RLC). One important result is a list of the modal resonances of the antenna, which gives deeper knowledge of its response to incident radiation. We now know how to design antenna structures with optimized characteristics and how to improve designs to work under different conditions. This richness in understanding is still percolating to the higher frequencies, in part because we have only recently learned how to construct structures small enough to resonate in this region, and partly because metal does not perform in the optical region (OR) like it does in the RF, due to strong dispersion and loss at these frequencies.

Applying antenna theory effectively in the near infrared (NIR) and OR is important,¹ because research in negative-index meta-materials, single photon emitters,² wireless optical broadcasting links,³ bio-sensors,⁴ and light capture in solar cells^{5,6} are all beginning to consider more and more complicated metallic nano-structures in these regions. As with antennas in the RF, the key function to obtain for nano-scale structures is the input impedance. Four methods have been developed:⁷ (1) the boundary-value method, (2) the

transmission-line method, (3) the Poynting vector method, and (4) the integral equation method. Much progress has already occurred in this endeavor. By extending the standard Pocklington integral equation to the optical region, for example, Alu and Engheta,⁸ DeAngelis *et al.*,⁹ and Locatelli *et al.*¹⁰ derived surface impedance functions for the dipole. Indeed, Hanson¹¹ developed the classical radiation efficiency of the dipole in the high gigahertz (GHz) and low terahertz (THz) regions using different metals. Alu and Engheta⁸ found the radiation efficiency and bandwidth for a nano-dipole and nano-dimer, both fed by nano-transmission lines. Less rigorous, but nevertheless effective, methods have been used to derive impedance functions for bulk, single-surface, and parallel-plate plasmons.¹² Using these new methods, which include the calculation of a "kinetic inductance" and "coupling capacitance" or "gap capacitance" for simple LC models, Delgado *et al.*¹³ and Corrigan *et al.*¹⁴ derived the resonances of circular and square loops. All of this effort to extend RF techniques to the OR is still in its infancy, and further development promises to enhance our understanding of complex antenna geometries.

Over the past decade, researchers have discovered that the resonances of circular, square, and hexagonal loops are particularly easy to change by modifying their diameter and thickness and by introducing gaps in the circumference. Many have explained this behavior with simplified RLC models^{13,15–20} and by using plasmonic fluid flow equations,²¹ but the methods do not use standard antenna theory. Finally, some researchers have calculated and identified experimentally the resonance saturation of loops,^{22–29} but again using simplified LC models.

In this paper, we provide a derivation of the input impedance for circular loops in the NIR and OR from standard

^{a)}Electronic mail: arni.mckinley@gmail.com

antenna theory. It takes into account the material characteristics of the wire from which the loop is constructed. This is an extension of an earlier work, which formulated the input impedance in the RF region as a RLC circuit representation.³⁰ In that work, we showed that the results also extended to the high GHz regime. In order to extend the RLC model to the NIR and OR, we derive additional terms, so that the modal RLC elements of circular loops, constructed of metals, dielectrics, or semi-conductors can now be calculated at any wavelength from the RF through the OR. We present an approximate function that gives all of the modal resonances of the loop as a function of its circumference; resonance saturation is clearly evident as a result. We also show by the use of simulations that these effects extend to hexagonal and square loops.

In Sec. II, we revisit classical theory of the circular loop at long wavelengths. In Sec. III, we extend the theory to the NIR and OR, showing how the input impedance changes as a function of material characteristics, and we specify modifications to the RLC model of the loop. We also verify the analytic theory using numerical simulations. In Sec. IV, we present results, including calculations of resonance saturation, current distribution, quality factor, radiation resistance, ohmic loss, and radiation efficiency. Section V gives a comparison with the experimental literature.

II. A REVIEW OF CLOSED LOOP THEORY AT LOW FREQUENCIES

The parameters of the circular loop are shown in Fig. 1(a). An analytic form for its input impedance has been known since the mid-1950s.^{31,32} In a recent paper,³⁰ we derived a simplified form by recasting the formulation as a RLC model. We showed that the loop looks like an infinite set of series resonant circuits in parallel

$$Z = 1 / \left[\frac{1}{Z_0} + \sum_1^{\infty} \frac{1}{Z_m} \right], \quad (1)$$

where each series modal impedance is given by

$$Z_0 = i\pi\zeta_0 a_0 \text{ and } Z_m = i\pi\zeta_0 (a_m/2). \quad (2)$$

The coefficients a_0 and a_m are functions of frequency and include integrals of Bessel functions. $\zeta_0 \approx 377 \Omega$ is the impedance of free space. A RLC representation of (1) appears in Fig. 1(b).

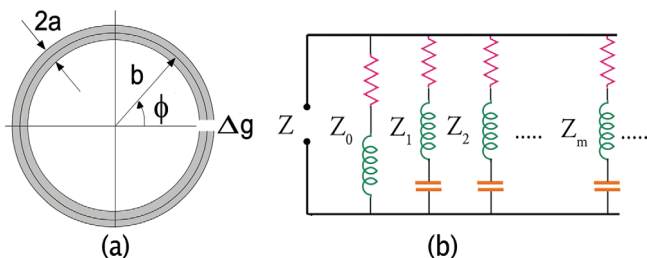


FIG. 1. (a) Geometry of the classical loop antenna, showing the key variables. The gap is infinitesimal and supports a “delta-function” driving voltage. (b) The RLC model of a closed circular loop antenna in standard form.

Equation (2) may be reformed to show the R, L, and C used in each modal circuit

$$Z_m = R_m + i \left(\omega L_m - \frac{1}{\omega C_m} \right) = \xi_0 \left[\left(k_b r_m - \frac{m^2}{k_b g_m} \right) + i \left(k_b l_{\mu m} - \frac{m^2}{k_b l_{\epsilon m}} \right) \right], \quad (3)$$

where r_m , g_m , $l_{\mu m}$, and $l_{\epsilon m}$ are unit-less functions of k_b given in Ref. 30, and

$$\begin{aligned} R_m &= \xi_0 (k_b r_m - m^2 / (k_b g_m)) \\ L_m &= \mu_0 b l_{\mu m} \\ C_m &= \epsilon_0 b l_{\epsilon m} / m^2. \end{aligned} \quad (4)$$

The term k_b is the propagation constant of waves in free space multiplied by the radius of the loop

$$k_b = \omega b / c = 2\pi b / \lambda = (\text{loop circumference}) / \lambda.$$

It compares the circumference of the loop to the free-space driving wavelength. μ_0 is the permeability and ϵ_0 the permittivity of free space. A sizing parameter, $\Omega = 2\ln(2\pi b/a)$, is typically used in the low frequency literature; the larger Ω , the thinner the loop.

A plot of (1) for a thin loop in the RF and MW regions appears in Fig. 2. The loop resonates when the reactance goes to zero. These “zero-crossings” (ZC) are of two types: (1) resonances, where the current wave exactly reinforces itself as it traverses the circumference, usually near integer multiples of the circumference, i.e., $\lambda = m \times 2\pi b$; and (2) anti-resonances, where the current wave exactly cancels itself, usually occurring near half integer multiples of the circumference ($\lambda = m/2 \times 2\pi b$). Both are important because, at a resonance, the loop can accumulate and store energy, while at an anti-resonance, it rejects incident energy. Reactance plots of thicker loops suggest that as loops

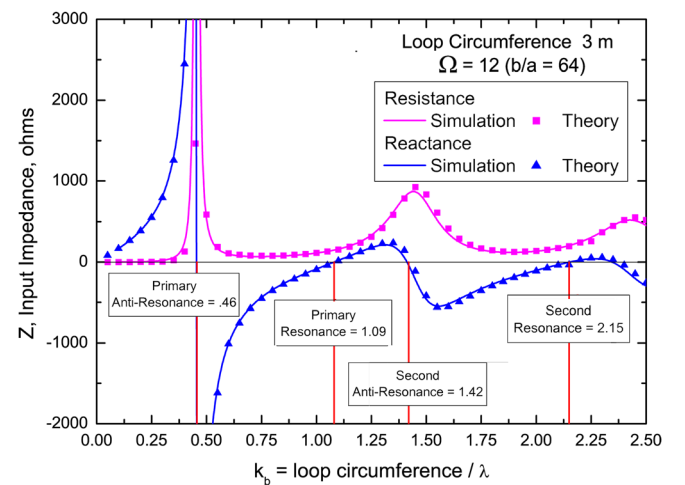


FIG. 2. Plot of the input impedance for a thin loop ($\Omega = 12$; $b/a = 64$) with a circumference of 3 m. The first two zero-crossing resonances and anti-resonances can be identified. These results apply to any perfectly conducting closed loop where $2\pi b > 3$ mm in the region $0 < k_b < 2.5$, since the material characteristics do not affect the impedance.

thicken, they tend to lose their zero-crossings except for the first ZC anti-resonance.

Equally important are the loop's modal harmonic resonances, of which there are an infinite number. These occur near, but are not identical with, the ZC resonances. They are important because current in the loop peaks at the modal resonances, rather than at the ZC resonances; one would therefore design to these resonances for better radiation efficiency.

Using (4), these modal resonances are found by solving

$$\omega_{mr} = \sqrt{1/(L_m C_m)} = \frac{mc}{b\sqrt{l_{\mu m} l_{\epsilon m}}} \quad \text{or} \quad k_{bmr} = \frac{2\pi b}{\lambda_{mr}} = \frac{m}{\sqrt{l_{\mu m} l_{\epsilon m}}}. \quad (5)$$

Our earlier paper showed how to solve this implicit function for all of the modal resonances. The key point is that the modal RLC elements are not constant with k_b and any model that treats them as constant is over-simplified. Figure 3, for example, shows the variation of the resistance, inductive reactance, and capacitive reactance for mode 0 through mode 2 as a function of k_b for a given loop

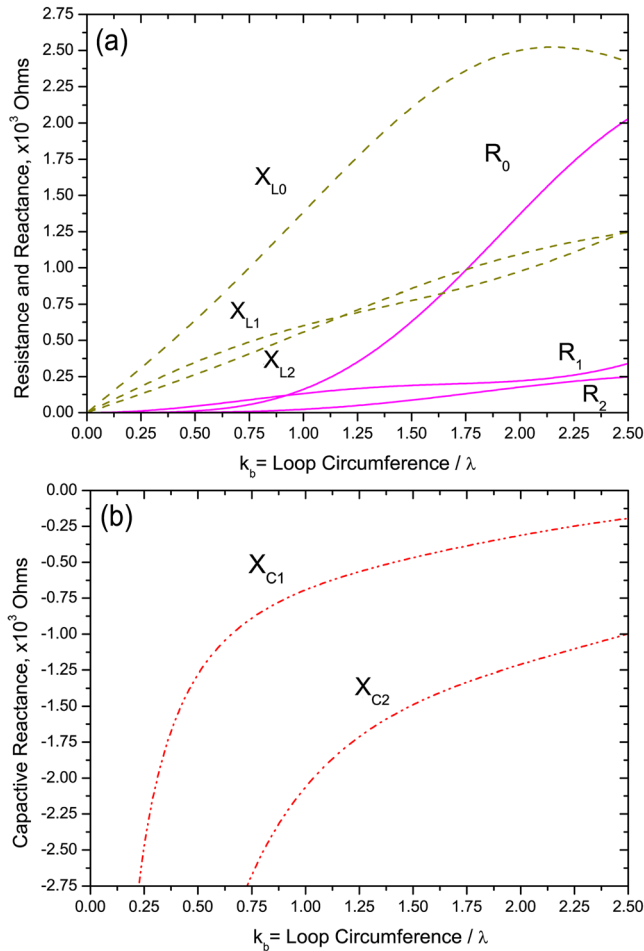


FIG. 3. (a) The resistance (R_m) and inductive reactance ($X_{Lm} = \omega L_m$) and (b) the capacitive reactance ($X_{Cm} = -1/(\omega C_m)$), for the zero-order and first two modes for a size $\Omega = 10$ ($b/a = 24$) loop. There is no zero mode capacitance. These results apply to perfectly conducting closed loops longer than 3 mm.

circumference. Equation (4) applies to such loops where the circumference is longer than 3 mm and $0 < k_b < 2.5$.

III. EXTENSION TO THE NEAR INFRARED AND OPTICAL REGION

A. Derivation from first principles

In this section, we derive the input impedance of a circular loop in the optical region. The governing equation comes directly from Maxwell's equations in cylindrical coordinates. An extra optical term is added to account for the dispersive properties of the material, and the equation is solved for the current. The input impedance is defined as the voltage divided by the current at an infinitesimal gap placed in the loop where excitation is applied. The behavior of the loop in the OR differs from that in the RF because of wavelength scaling, a phenomenon caused by the dispersive properties of metals in this region.

King³³ summarizes Storer's³¹ and Wu's³² derivation of the input impedance function in the RF and except for inclusion of the material characteristics, we follow it exactly for the OR derivation. A delta function voltage generator, $V_0\delta(\phi)$, is located across an infinitesimal gap at $\phi = 0$ (see Fig. 1). The delta function requires $E_\phi = 0$ except at $\phi = 0$, where it becomes infinite, but in such a manner that

$$\int_{-\Delta g/2}^{\Delta g/2} E_\phi b d\phi = -V_0, \quad (6)$$

where b is the radius of the loop and Δg is the width of the gap.

This imposed electric field generates a scalar potential, Φ and a vector potential, \vec{A} , according to $\vec{E} = -\nabla\Phi - \partial\vec{A}/\partial t$. This causes a current in the loop which induces a voltage drop across the characteristic impedance of the metal, Z_s . This impedance is due to the material characteristics. Expanding in cylindrical coordinates, and using $\exp(i\omega t)$, gives

$$\frac{V_0\delta(\phi)}{b} - J_\phi(\phi)Z_s = \frac{1}{b} \frac{\partial\Phi}{\partial\phi} + i\omega A_\phi, \quad (7)$$

$J_\phi(\phi)$ is a current density distributed on the surface^{9,10,34–36}

$$J_\phi(\phi) = J_s(\phi)\delta(\rho - a) = \frac{I(\phi)\delta(\rho - a)}{2\pi a}. \quad (8)$$

In a perfectly conducting wire, the current moves everywhere to create an electric field which exactly cancels any imposed electric field. Therefore, the driving field, E_ϕ , appears only in the gap. As a result, a boundary condition for the solution of Eq. (7) is that the total electric field, given by the sum of the imposed field and the reactive field, is zero on the surface of the wire; i.e., $Z_s = 0$.

In an imperfectly conducting wire, this is not the case; the surface current produces an E_ϕ field through the wire, across the wire impedance, $J_\phi Z_s$. The propagation vector has not only a primary component in the transverse direction but also a component in the axial direction which grows larger as the wavelength approaches the IR. This raises several difficulties in the solution of Eq. (7). An assumption that the

wire is thin, $a^2 \ll b^2$, forces the axial component to zero, and allows a simpler solution. Applying the solution to thicker loops, therefore, will be less accurate than an application to thinner loops. Moreover, applying the solution in the IR and OR will also be less accurate.

From hereon, the derivation follows King³³ precisely and the result for the current is

$$I(\phi) = \sum_{-\infty}^{\infty} \left[\frac{V_0}{i2\pi\xi_0 a_m/2 + (b/a)Z_s} \right] e^{-im\phi} \\ = V_0 \left[\frac{1}{i\pi\xi_0 a_0 + (b/a)Z_s} + \sum_{m=1}^{\infty} \frac{2\cos(m\phi)}{i\pi\xi_0 a_m + (b/a)Z_s} \right]. \quad (9)$$

The input impedance at the gap becomes

$$Z = \frac{V_0}{I(\phi=0)}, \\ = 1 / \left[\frac{1}{i\pi\xi_0 a_0 + (b/a)Z_s} + \sum_{m=1}^{\infty} \frac{1}{i\pi\xi_0 (a_m/2) + (b/a)(Z_s/2)} \right], \\ = 1 / \left[\frac{1}{Z'_0} + \sum_{m=1}^{\infty} \frac{1}{Z'_m} \right], \quad (10)$$

where

$$Z'_0 = i\pi\xi_0 a_0 + (b/a)Z_s \\ Z'_m = i\pi\xi_0 (a_m/2) + (b/a)(Z_s/2). \quad (11)$$

The difference between Eqs. (2) and (11) is an extra term that depends on the wire impedance, Z_s . The a_0 and a_m coefficients are given by King and can be found in our previous paper.³⁰ The functional character of Z_s remains to be determined.

B. The surface and characteristic wire impedance

The impedance, Z_s , is required to go to zero at low frequencies and to play a significant role in the mode summation at optical frequencies.

A cylindrical wire, made of an imperfectly conducting material, propagates an electromagnetic field inside that can be described well using Bessel functions of the first kind. The field external to the wire uses Hankel functions. Derivations are shown in Stratton³⁷ and Hanson.¹¹ Novotny³⁸ uses the same approach to derive a theory of wavelength scaling in dipoles. Stratton and Hanson give the surface impedance of a cylindrical wire as

$$z_s = \frac{\gamma}{2\pi a \sigma} \frac{J_0(\gamma a)}{J_1(\gamma a)}$$

in Ω/m , γ is the transverse propagation constant in the wire, and $J_0(\gamma a)$ and $J_1(\gamma a)$ are the zero and first order Bessel functions of the First Kind. We have already included the wire circumference $2\pi a$ in (8), and therefore, for the characteristic wire impedance in ohms, we use

$$Z_s = \frac{\gamma J_0(\gamma a)}{\sigma J_1(\gamma a)}. \quad (12)$$

Under these assumptions, the conductivity is directly related to the index of refraction, $\eta = n - i\kappa$

$$\gamma = \frac{\omega}{c} \eta \quad \text{and} \quad \sigma = i\omega\epsilon_0(\eta^2 - 1), \\ \frac{\gamma}{\sigma} = -i\xi_0 \frac{\eta}{\eta^2 - 1}, \quad (13) \\ Z_s = -i\xi_0 \frac{\eta}{\eta^2 - 1} \frac{J_0(\gamma a)}{J_1(\gamma a)}.$$

C. Modeling the index of refraction

The conductivity of any material is, in general, complex and can vary dramatically over the full range of frequencies from DC to the visible. The magnitude of the conductivity of gold, in particular, begins at 45×10^6 S/m at DC, then falls off by a factor of 30 between $\lambda = 1.5$ mm in the MW and $2 \mu\text{m}$ in the infrared, where the first measured index by Johnson and Christy³⁹ occurs. The imaginary part dominates the real from $100 \mu\text{m}$ until the onset of the inter-band and intra-band transitions in the middle of the visible region (about 500 nm), where the real part again dominates and gold picks up its yellowish color.

The decrease in conductivity is due to Drude's behavior, and in fact Drude's model provides a reasonable representation of the permittivity to the onset of the transition bands. Since the permittivity is the square of the index of refraction, and since the conductivity is directly related to the index, it is possible to develop a Drude-like model for the index itself. However, it must be extended to include the critical points of the band transitions. Several models appear in the literature to do that. Etchegoin *et al.*^{40,41} and Vial and Larouche⁴² are recent examples. The transitions appear in the models as a summation of Lorentzian resonances where the critical transitions occur. We extend the model by Etchegoin's group in such a way as to ensure that both the index data by Johnson and Christy and the DC conductivity of the metal are satisfied

$$\eta^2 = 1 - \frac{f_0 \omega_p^2}{\omega} \left(\frac{1}{(\omega - i2\Gamma_0)} + \frac{\alpha}{(\omega - i2\beta\Gamma_0)} \right) \\ + \sum_{m=1}^{\infty} \frac{f_m \omega_p^2}{2\omega_m} \left[\frac{e^{i\pi/\gamma_m}}{\omega_m - \omega + i\Gamma_m} + \frac{e^{-i\pi/\gamma_m}}{\omega_m + \omega - i\Gamma_m} \right], \quad (14)$$

where ω_p is the metal's plasma frequency, f_n are the quantum probabilities of transition, ω_m are the critical points, and Γ_m are the Lorentz broadening terms for the transitions. Using (14), the DC value of the conductivity is

$$\sigma_0 = \frac{f_0 \omega_p^2 \epsilon_0}{2\Gamma_0} \left[1 + \frac{\alpha}{\beta} \right]. \quad (15)$$

Note that the Johnson and Christy data assume a $\exp(-i\omega t)$ dependence, instead of $\exp(i\omega t)$ as we used, and therefore, their index, $\eta = n + i\kappa$, is the complex conjugate of that delivered by our model. Table I gives the parameter values for gold, silver, and copper. With the proper parameters, (14) is also a good model for many semi-conductor materials.

TABLE I. Parameter fits for (14) for gold, silver, and copper.

| | $\sigma_0 \times 10^6$ (Ω/m) | α | β | f_0 | Γ_0 (eV) | f_1 | ω_1 (eV) | γ_1 | Γ_1 |
|----|---|--------------------|------------|--------------------|--------------------|--------------------|--------------------|--------------------|--------------------|
| Au | 45 | 1.540 | 13.180 | 0.37 | 0.005 | 0.20 | 2.62 | 4.00 | 0.60 |
| Ag | 63 | 0.100 | 0.350 | 0.94 | 0.010 | 0.14 | 4.32 | 4.62 | 0.34 |
| Cu | 60 | 0.035 | 0.005 | 1.00 | 0.064 | 0.23 | 2.30 | 3.53 | 0.52 |
| | f_2 | ω_2 (eV) | γ_2 | Γ_2 (eV) | f_3 | ω_3 (eV) | γ_3 | Γ_3 (eV) | ω_p (eV) |
| Au | 0.35 | 3.70 | 4.00 | 1.10 | 0.60 | 7.00 | 4.00 | 2.20 | 9.0 |
| Ag | 0.45 | 5.50 | 12.32 | 1.40 | 0.40 | 7.53 | 4.00 | 2.10 | 9.0 |
| Cu | 0.22 | 3.14 | 2.56 | 0.95 | 0.32 | 4.87 | 2.70 | 1.10 | 8.4 |

Figure 4 shows the real and imaginary parts of the wire impedance of a thin gold loop ($\Omega = 12$) given by (13) for three different circumference lengths in the NIR and OR. The principal reason for the sudden increases in the curves is the effect of the transition bands on the Bessel function ratio, $J_0(\gamma a)/J_1(\gamma a)$. The figure tells us that the degree to which a given loop is affected by the transitions depends on its circumference and the driving wavelength. Different sized loops respond to the same driving wavelength differently. For example, a 600 nm circumference loop will be affected

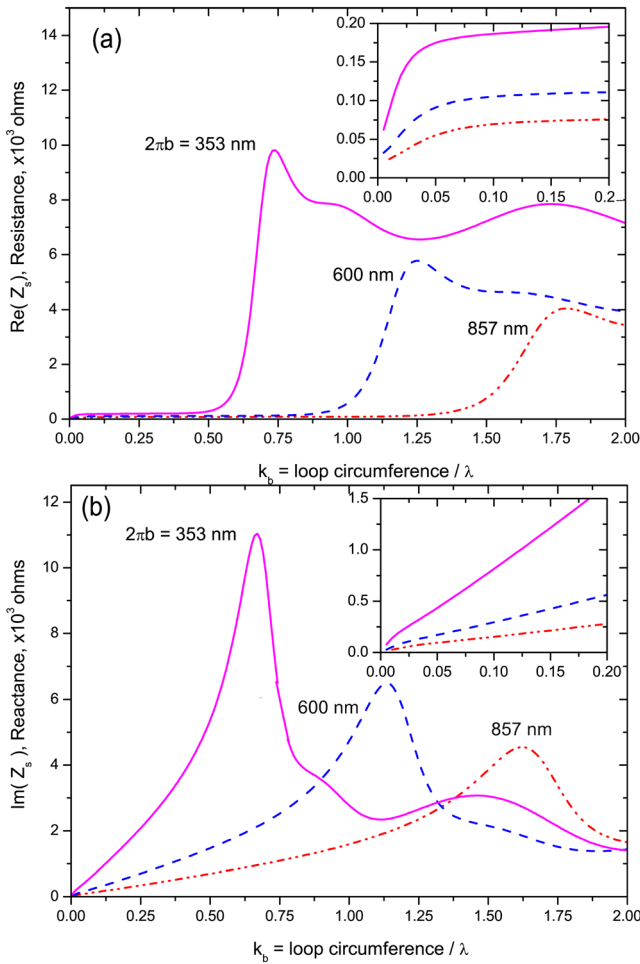


FIG. 4. The characteristic wire impedance, Z_s , of a thin loop ($\Omega = 12$; $b/a = 64$) for three circumferences in the OR, from (13); (a) resistance and (b) reactance. The inset shows the region where closed loops resonate: $0.05 < k_b < 0.2$. Thicker loops show smaller values.

by the transitions when the driving wavelength reaches the length of the circumference, at 600 nm. But a 353 nm loop will be affected when the driving wavelength reaches double its circumference, at 700 nm. In any case, resonance saturation puts all of the modal resonances of such loops outside transition effects. We show in Sec. IV B that at optical circumferences, these loops resonate in the region $k_b \leq 0.2$, shown by the insets.

D. The RLC model in the optical region

In our previous paper,³⁰ we presented an exact RLC model for the perfectly conducting closed loop. That model may be applied to any thickness loop in the region $0 < k_b < 2.5$. Difficulties arise for loops when material characteristics affect electron mobility. Analytically, the argument of the Bessel functions in (13) involves the index of refraction and this makes a derivation of an exact RLC model for the optical regime impossible. However, an approximate analytical form is easily found by assuming $\gamma a \ll 1$. Taking the Bessel functions to first order⁴³ in γa , we have

$$\frac{J_0(\gamma a)}{J_1(\gamma a)} \approx \frac{1 - (\gamma a)^2/4}{(\gamma a)/2}. \quad (16)$$

Substituting into (13), the optical term, $b/a \times Z_s$, can be approximated as

$$\begin{aligned} \frac{b}{a} Z_s &= \frac{\xi_0}{|\eta^2 - 1|^2} \\ &\times \left[\left(\frac{k_b}{2} + \frac{2(b/a)^2}{k_b} \right) \text{Im}(\eta^2) + i \frac{k_b}{2} (|\eta^2|^2 - \text{Re}(\eta^2)) \right] \\ &+ i \frac{\xi_0}{|\eta^2 - 1|^2} \left[\frac{2(b/a)^2}{k_b} (1 - \text{Re}(\eta^2)) \right] \\ &= \xi_0 \left[\left(k_b r_s - \frac{1}{k_b g_s} \right) + i \left(k_b l_{\mu s} - \frac{1}{k_b l_{\epsilon s}} \right) \right]. \end{aligned} \quad (17)$$

Using (10) and the definitions

$$\begin{aligned} R'_m &\equiv \xi_o \left[k_b (r_m + r_{sm}) - \frac{1}{k_b} \left(\frac{m^2}{g_m} + \frac{1}{g_{sm}} \right) \right], \\ L'_m &\equiv \mu_o b (l_{\mu m} + l_{\mu sm}), \\ C'_m &\equiv \epsilon_o b \frac{1}{(m^2/l_{\epsilon m} + 1/l_{\epsilon sm})}, \end{aligned}$$

the modal input impedance in (10) becomes approximately

$$\begin{aligned} Z'_m &\approx R'_m + i \left(\omega L'_m - \frac{1}{\omega C'_m} \right) \\ &= \xi_o \left(k_b (r_m + r_{sm}) - \frac{1}{k_b} \left(\frac{m^2}{g_m} + \frac{1}{g_{sm}} \right) \right) \\ &+ i \xi_o \left(k_b (l_{\mu m} + l_{\mu sm}) - \frac{1}{k_b} \left(\frac{m^2}{l_{\epsilon m}} + \frac{1}{l_{\epsilon sm}} \right) \right), \end{aligned} \quad (18)$$

where

$$r_{sm} = \begin{cases} \text{Im}(\eta^2)/(4|\eta^2 - 1|^2) & \text{if } m > 0 \\ \text{Im}(\eta^2)/(2|\eta^2 - 1|^2) & \text{if } m = 0, \end{cases}$$

$$g_{sm} = \begin{cases} -|\eta^2 - 1|^2/((b/a)^2 \text{Im}(\eta^2)) & \text{if } m > 0 \\ -|\eta^2 - 1|^2/(2(b/a)^2 \text{Im}(\eta^2)) & \text{if } m = 0, \end{cases}$$

$$l_{\mu sm} = \begin{cases} (|\eta^2|^2 - \text{Re}(\eta^2))/(4|\eta^2 - 1|^2) & \text{if } m > 0 \\ (|\eta^2|^2 - \text{Re}(\eta^2))/(2|\eta^2 - 1|^2) & \text{if } m = 0, \end{cases}$$

$$l_{esm} = \begin{cases} -|\eta^2 - 1|^2/((b/a)^2(1 - \text{Re}(\eta^2))) & \text{if } m > 0 \\ -|\eta^2 - 1|^2/(2(b/a)^2(1 - \text{Re}(\eta^2))) & \text{if } m = 0. \end{cases}$$

Since the index of refraction is wavelength dependent, it is not sufficient to specify only a value for k_b in order to calculate the modal RLC elements. One must specify a circumference as well. Fig. 5 compares the reactance of (10) using the exact Z_s term (12) and using the approximate Z_s term (18) for various circumferences of a thin loop, $\Omega = 12$ ($b/a = 64$). For circumferences larger than 20–30 μm , the approximate reactance in (18) is a poor fit with the exact result given by (12). But for 6 μm and shorter, the agreement is very good. Therefore, any calculations with the approximation (16) can be applied to loops with circumferences shorter than about 10 μm .

E. Simulation verification

Figures 2, 6, and 7 show the input impedances for three gold nano-loops with different circumference lengths, one in the GHz region, one in the NIR, and one in the OR, as given by (10) and by simulation using CST Microwave StudioTM (MWS).⁴⁴ The accuracy of the analytic model depends to some extent on the handling of the infinite summation of (10). In our previous paper,³⁰ we followed Storer's approach³¹ by summing to the fourth mode, then adding an extra term to account for the effect of the higher modes. This is a valid approach for the RF, but optical loops require more

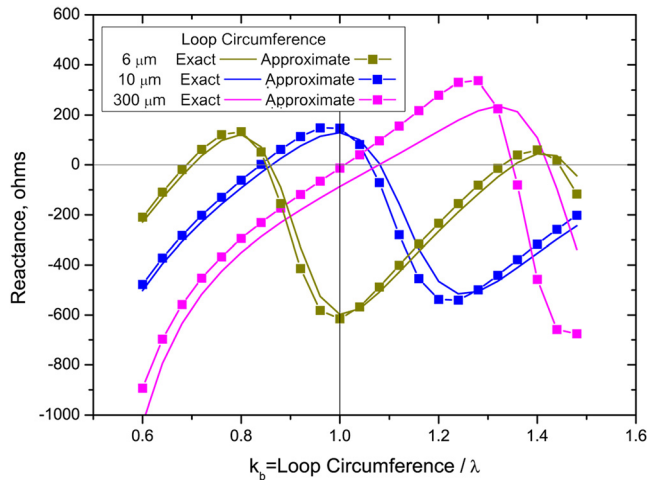


FIG. 5. The reactance for three gold thin loops ($\Omega = 12$; $b/a = 64$) of differing circumferences, comparing the effect of the exact optical term (12) with the approximate (17). The smaller the loop, the more exact the optical term approximation becomes.

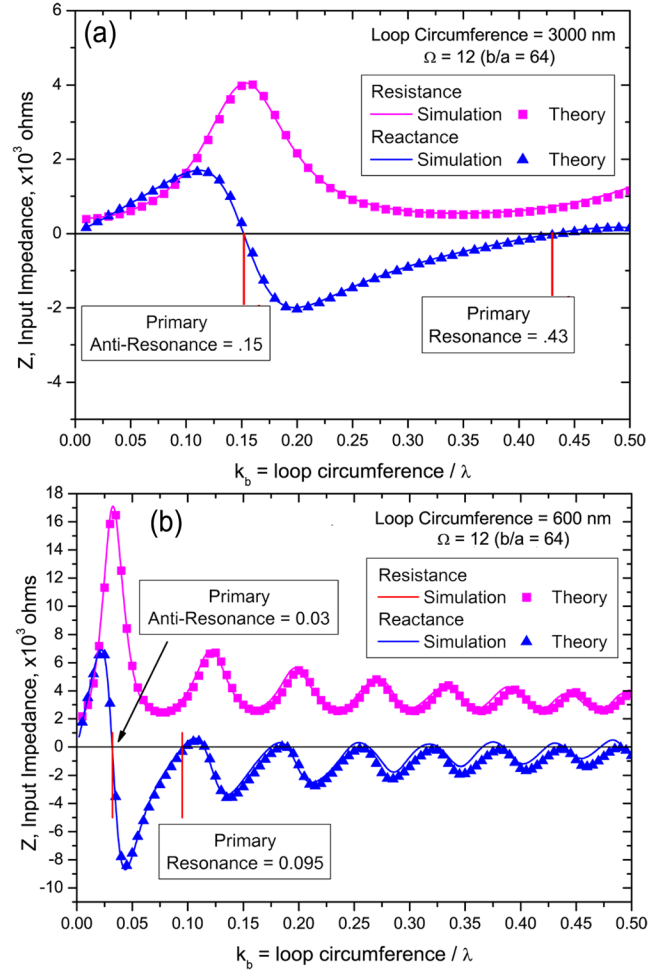


FIG. 6. Verification of Theory: Impedance for two circular thin loops, calculated from (10) compared with numerical simulations. (a) $2\pi b = 3000$ nm and (b) $2\pi b = 600$ nm.

summation terms. To obtain the results in Figs. 2, 6, and 7, we elected to sum the first 30 modes and then added only a portion (25%) of Storer's extra term. This was selected by fitting the simulation data to the theory for the entire

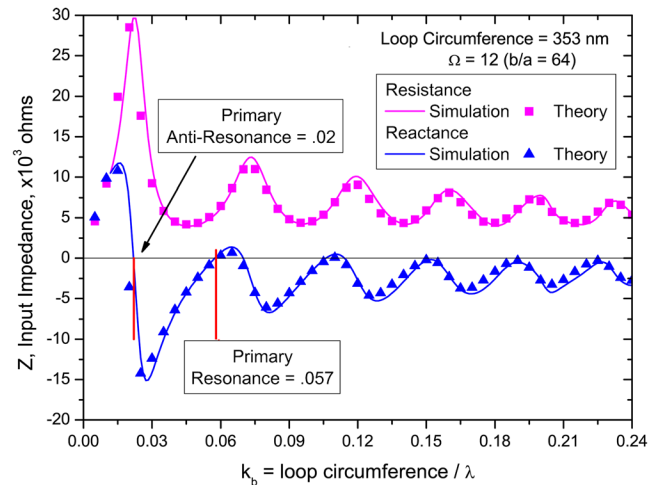


FIG. 7. Verification of theory (expanded axis): The impedance of a circular thin loop of circumference is 353 nm. The first ZC resonance is at $353/0.057 = 6192$ nm.

frequency range from RF to OR. The match between theory and numerical simulation is very close for all three loops. The analytic theory assumes a thin loop, so thicker loops will not show as close an agreement.³⁰ We show a comparison with the experimental literature for thick loops in Sec. V.

IV. RESULTS

A. Optical impedance of the circular loop

An examination of Figs. 2, 6, and 7 shows that the extra optical term in (11) causes the input impedance function to compress; all resonances migrate toward wavelengths longer than the circumference. Three points are important: (1) the shape of the functions is essentially the same; (2) the zero crossings migrate; and (3) the magnitude of the impedance increases with shorter circumferences. The first point means that all loops respond similarly to incident energy. The second means that the ZC resonances move toward smaller values of k_b as the circumference decreases; the ZC resonances must therefore eventually saturate. The third means that smaller loops carry smaller current magnitudes and lag the driving field.

In Fig. 6(b), notice that although the loop circumference matches a wavelength in the mid-visible region, the loop's first ZC resonance is at $600/0.095 = 6316$ nm, well outside the OR. However, the highest resonance shown occurs at $600/0.5 = 1.2$ μm .

B. Resonance saturation of loops in the optical region

Several authors^{22,24,26,38,45} have noticed that as dipoles and loops are made shorter, they tend to resonate at wavelengths longer than their lengths or circumferences would suggest. Indeed, they eventually reach a minimum wavelength below which they will not resonate. Our model gives an accurate functional curve for this behavior in loops. The reason is the extra optical term in (11).

Using the approximation (18), we can derive an equivalent expression to (5), which gives the modal resonances in the OR

$$k_{bmr} = \frac{2\pi b}{\lambda_{mr}} = \sqrt{\frac{m^2 + l_{em}/l_{esm}}{l_{em}l_{\mu m} + l_{em}l_{\mu sm}}}. \quad (19)$$

Since this assumes the small γa approximation, it applies only to loops with circumferences less than 10 μm . It is also less accurate for loops of thickness $\Omega \leq 7$ (that is, for $b/a \leq 5.3$). $l_{\mu m}$ and l_{em} are the low frequency, unit-less, functions related to the loop inductance and capacitance, respectively, found in our previous paper.³⁰ $l_{\mu sm}$ and l_{esm} are the high frequency additions coming from the new optical term. Figure 8 shows a plot of (19) for loops of various thicknesses, compared with data taken from simulations. The theory is less accurate for thick loops, because of the assumption that $a^2 \ll b^2$. Even so, the analytic model matches numerical simulations down to thicknesses of $\Omega = 8$ ($b/a = 8.7$). We see immediately a resonance saturation for each loop. The cutoff for the thinnest loop is about 6.2 μm , below which closed, gold nano-loops will have no

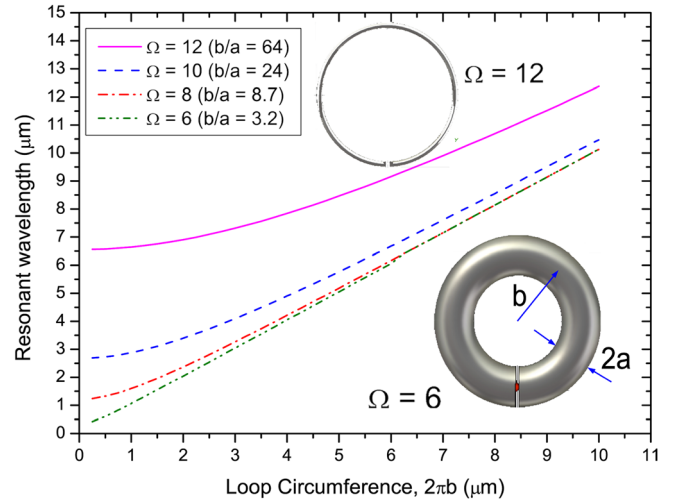


FIG. 8. The first modal resonance ($m = 1$) as a function of the circumference for four gold loops of various thicknesses, given by (5). All loops show cut-offs in the near infrared, except the thickest.

first harmonic ($m = 1$) resonance. Theory predicts a cutoff for the thickest loop of about 600 nm, but the simulations put it at about 1.0 μm .

Resonance saturation occurs for hexagons and squares as well. Figure 9 shows ZC resonances for simulated circular, hexagonal, and square loops, compared with the ZC resonances identified from numerical input impedance plots of circular loops using (10). The radius of the wire, a , for these loops is taken to be the radius of a circumscribing circle through the middle of the wire at the corners. The circle circumscribing the hexagon or square itself has radius b . We conclude that the shape of the loop is not an important parameter for saturation.

C. Current, quality factor, radiation resistance, ohmic loss, and radiation efficiency of optical loops

The distribution of current on a circular loop in the OR is given by (9) and (10) with $V_0 = 1$. It is composed of a

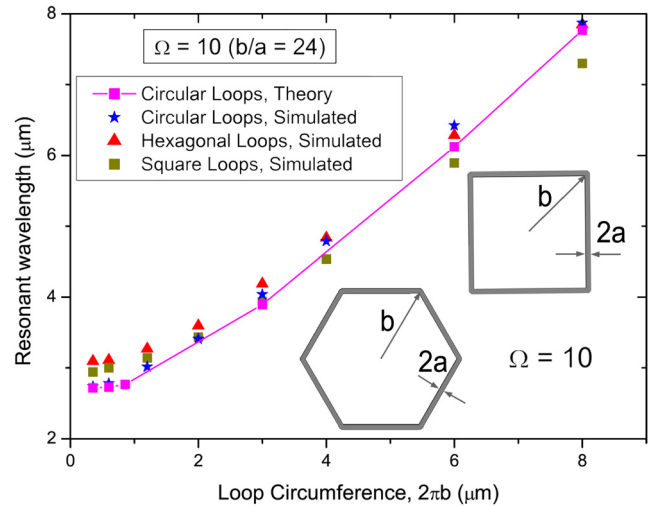


FIG. 9. The first ZC resonances of simulated gold circular, hexagonal, and square nano-loops of size $\Omega = 10$ ($b/a = 24$) compared with ZC resonances measured from plots using (10). The line joins the points calculated from (10) as a guide to the eye.

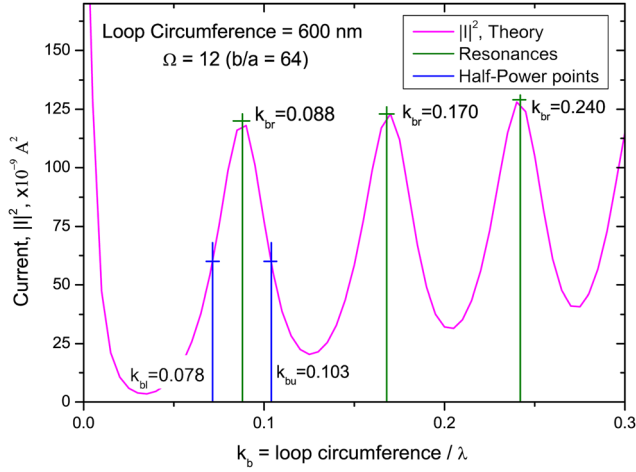


FIG. 10. The squared magnitude of the current as a function of k_b for a gold loop of circumference of 600 nm. The first, second, and third harmonic peaks are marked. The upper and lower half-power points of the first peak are also marked.

zero-order DC current and *cosine* terms associated with each mode. Figure 10 shows the current magnitude at $\phi = 0$ for a 600 nm circumference loop as a function of k_b . The first ZC resonance occurs at $k_b \approx 0.1$, but the current peak occurs at $k_b \approx 0.09$. This slight discrepancy occurs for all loops, even at long wavelengths, as Table II shows. Interestingly, the table also shows that the current peaks occur at the *modal* resonances. This is important because loops radiate best where the current is high, consequently one should design to the modal resonances, not the ZC resonances. Moreover, since there are high peaks at many modes for thin loops, such loops will radiate at many harmonics. This is one reason why loops are not used for communication in the RF region. Since the modal resonances for thicker loops overlap more than in thin loops, their current peaks are not as pronounced and their current peaks are smaller and broader.

The high current in the very low k_b region is due to the zero-order term in (9). The peak and half power points can be directly measured from the curve, which allows a calculation of the loop's modal quality factor. Q is calculated using $k_{br}/(k_{bu} - k_{bl})$, where "u" and "l" refer to the upper and

TABLE II. Zero-crossing resonances from (10), modal resonances from (19), and squared current peaks from (9) at $\phi = 0$ for thin gold closed loops. This table shows that the current peaks occur at the modal resonances rather than at the ZCs.

| $\Omega = 12$ | Resonance #1 | | | Resonance #2 | | |
|--|--------------|----------------|-----------------------|--------------|----------------|-----------------------|
| | ZC k_b | m = 1 k_b | $ I ^2$ Peak k_b | ZC k_b | m = 2 k_b | $ I ^2$ Peak k_b |
| $2\pi b$ μm ≥ 3000 | 1.09 | 1.07 | 1.04 | 2.15 | 2.10 | 2.15 |
| 10.00 | 0.86 | 0.81 | 0.80 | 1.70 | 1.59 | 1.60 |
| 8.00 | 0.80 | 0.75 | 0.73 | 1.56 | 1.47 | 1.47 |
| 6.00 | 0.70 | 0.66 | 0.64 | 1.35 | 1.28 | 1.28 |
| 3.00 | 0.43 | 0.41 | 0.40 | 0.83 | 0.79 | 0.78 |
| 0.86 | 0.14 | 0.13 | 0.13 | 0.26 | 0.24 | 0.24 |
| 0.60 | 0.10 | 0.09 | 0.09 | 0.18 | 0.17 | 0.17 |
| 0.35 | 0.06 | 0.05 | 0.05 | 0.11 | 0.10 | 0.10 |

lower half power points, respectively. Table III shows the peak current magnitude and Q as a function of the circumference of the loop, taken from such calculations.

The radiation efficiency of the loop is the power radiated divided by power input. This leads to

$$\epsilon_{rad} = \frac{R_{rad}}{R_{rad} + R_{loss}}.$$

The radiation resistance is normally taken at the ZC resonance, since reactance goes to zero. However, since the current peak and the resonance are slightly different, and since one would construct a loop at the current peak, we will take the radiation resistance to be that at the k_b position of the peak, R_{res} , calculated by (10). Since there is additional loss in the optical region, the radiation resistance is $R_{rad} = R_{res} - R_{loss}$.¹⁰ The radiation efficiency, then, is

$$\epsilon_{rad} = \frac{R_{res} - R_{loss}}{R_{res}}.$$

We follow Hanson⁴⁶ in deriving R_{loss} from the ohmic power loss

$$P_{ohmic} = \frac{1}{2} R_{loss} |I_{in}|^2 = \frac{\text{Re}(Z_s)}{2} \int_0^{2\pi} |I(\phi)|^2 b d(\phi) \quad (20)$$

and therefore

$$R_{loss} = \frac{b \text{Re}(Z_s)}{a |I_{in}|^2} \frac{1}{2\pi} \int_0^{2\pi} |I(\phi)|^2 d(\phi).$$

TABLE III. Squared current peak, radiation resistance, ohmic loss, radiation efficiency, and quality factor of gold closed loops with varying circumferences, and sized $\Omega = 10$ and 12. All measures given for the first modal resonance of the loop. Note that the currents are calculated using $V_0 = 1.0$ in (10).

| $\Omega = 10$ | | | | | |
|---------------------------|--------------------------------------|-----------------------|------------------------|------------|-----|
| $2\pi b$ μm | $ I ^2 _{Pk}$ 10^{-6}A^2 | R_{rad} Ω | R_{loss} Ω | ϵ | Q |
| ≥ 3000 | 56.2 | 115 | 1 | 1.00 | 3.7 |
| 10.00 | 47.7 | 134 | 22 | 0.86 | 3.8 |
| 8.00 | 48.5 | 136 | 27 | 0.83 | 3.9 |
| 6.00 | 43.0 | 131 | 38 | 0.77 | 4.0 |
| 3.00 | 34.5 | 86 | 92 | 0.48 | 4.6 |
| 0.86 | 8.7 | 4 | 324 | 0.01 | 5.9 |
| 0.60 | 4.5 | 1 | 450 | 0.00 | 5.8 |
| 0.35 | 1.6 | 0 | 782 | 0.00 | 5.6 |
| $\Omega = 12$ | | | | | |
| ≥ 3000 | 52.0 | 128 | 0 | 1.00 | 5.0 |
| 10.00 | 15.4 | 81 | 150 | 0.35 | 3.5 |
| 8.00 | 11.9 | 76 | 193 | 0.28 | 3.3 |
| 6.00 | 8.20 | 59 | 262 | 0.19 | 3.2 |
| 3.00 | 2.70 | 32 | 537 | 0.06 | 3.0 |
| 0.86 | 2.40 | 10 | 1849 | 0.01 | 2.8 |
| 0.60 | 1.20 | 31 | 2563 | 0.01 | 2.7 |
| 0.35 | 0.40 | 21 | 4509 | 0.00 | 2.6 |

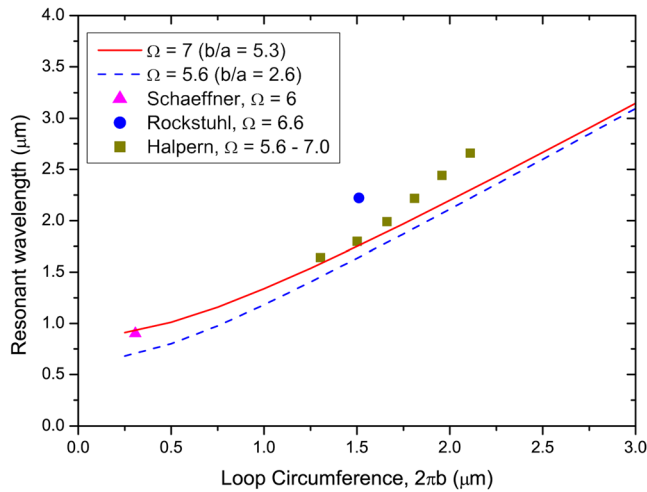


FIG. 11. A comparison of three studies from the literature with theory for loops of size $\Omega = 5.6$ to 7.

Table III gives a comparison of various measures for the loops of Table II at the first modal resonance for two thicknesses of wire. The thicker loop shows higher currents throughout the range, lower losses due to the thicker wire size, higher radiation efficiencies, and higher Q .

V. COMPARISON WITH THE LITERATURE

Most fabricated and measured loops are found in the meta-materials literature as square split-ring resonators (SRRs) and have gaps cut in the circumference of the loops. Recently, however, Halpern and Corn²⁹ have published a fast, low-cost fabrication technique in which the loop radius and wire radius are quite accurately fashioned. They fabricated gold, silver, and nickel loop arrays on glass substrates, and showed further that the loop resonances could be tuned by adjusting the loop radius and thickness. Figure 11 shows resonance peaks from absorbance spectra for gold loops with thicknesses between $\Omega = 5.6$ to 7. Despite the fact that these loops are in a large array on a substrate, the results fit our calculations well.

Schaffner⁴⁷ studied a gold circular loop fabricated on an ITO-glass substrate with a circumference of $0.31 \mu\text{m}$ ($b = 49 \text{ nm}$) and $a = 16 \text{ nm}$ ($\Omega = 6$). He shows a measured scattering response at $0.90 \mu\text{m}$.

Rockstuhl *et al.*⁴⁸ studied gold square loops on quartz substrate with sides of 400 nm and rectangular wire thickness of $60 \times 20 \text{ nm}$. An equivalent square loop in our measures is $a = 56.5 \text{ nm}$ and $b = 240 \text{ nm}$ ($\Omega = 6.6$). The circular circumference, therefore, is $1.5 \mu\text{m}$. They report a measured spectral reflectance peak at $2.2 \mu\text{m}$. The resonant wavelength of their square loop is red-shifted in Fig. 11 compared to theory, as would be expected from our comparison of loops shown in Fig. 9.

We note that all of these experimental results include the effect of substrates, which the analytical theory does not include.

VI. DISCUSSION

In general, closed loops follow the low frequency analytic theory, (1) through (5), with an extra term prominent in

each mode (see (9) and (10)). The extra term accounts for material dispersion at frequencies higher than the MW region, where electrons can no longer oscillate in phase with the incident energy. This slowing leads to wavelength scaling. The index of refraction completely accounts for these influences and appears prominently in this extra term. Careful modeling of the index is important, because the OR introduces inter-band and intra-band transitions that affect conductivity. We therefore use an extended Drude's model to compute the index.

For gold, the extra term begins to influence the input impedance and current calculation at loop circumferences shorter than 3 mm , but dominates by $10 \mu\text{m}$. The low frequency input impedance model leads to a RLC circuit representation of the loop, where element values are not constants, but rather functions of the circumference of the loop compared with driving wavelength, i.e., functions of $k_b = 2\pi b/\lambda$. As the driving wavelength reaches the MW regime, wavelength scaling sets in, and these RLC values also become functions of the index of refraction, which is inherently a function of wavelength.

The modal harmonic resonances are important, because the current peaks occur there, rather than at the zero-crossing resonances of the loop. All modal harmonic resonances saturate; the first mode ($m = 1$) saturates in the NIR for all loops thinner than $\Omega = 6$. The “roll-off” away from the linear slope toward saturation is rather abrupt, so that a rather large number of loop circumferences will give resonances at roughly the same wavelength (see Fig. 8).

The quality factor (Q) of thin gold loop antennas begins around 5 in the low frequencies and reduces as Drude's behavior sets in, until it saturates at about 2.5. Interestingly, the Q of thick gold loops increases from about 3.7 at long wavelengths to 5.5 at saturation. The radiation efficiency decreases dramatically for both thick and thin loops as the driving wavelength shortens, due to increased losses. These data imply that the performance of OR loops is substantially poorer than their performance at RF.

VII. CONCLUSION

We present an analytic theory of closed loop antennas from the RF through the OR, using standard antenna theory. This results in an exact function for the input impedance at all frequencies, an exact RLC representation at long wavelengths and an approximate RLC representation when the material characteristics of the wire influence behavior from about 3 mm into the OR. We provide an expression for the characteristic wire impedance, give values at example wavelengths, and show the effects this term has on loop resonances. We calculate the input impedance, modal harmonic resonances, current, current peaks, quality factor, radiation resistance, ohmic loss, and radiation efficiency. We show how to identify ZC resonances and ZC anti-resonances from the reactance of the loop. We also provide a useful model of the index of refraction for metals and semi-conductors, with parameter fittings for gold, silver and copper.

The analytic theory gives detailed behavior for circular loops up to the sizes and thicknesses of SRRs and loop arrays

currently being fabricated. The theory covers the RF, MW, low THz, NIR, and OR at least to 350 nm. Our work suggests that hexagonal and square loops also fit aspects of the theory, in particular, the effect of resonance scaling.

The theory takes standard antenna theory for loops in the RF and MW regimes and extends it to the nano-scale. As a result, it provides an understanding of how and why loops behave so differently in the NIR and OR. It provides a case study of using standard antenna tools in these regimes and consequently should provide a foundation for designing complex structures with enhanced reception and radiation at these short wavelengths.

ACKNOWLEDGMENTS

The corresponding author wishes to thank A. Basch and C. Barugkin from the Centre for Sustainable Energy Systems for reading the manuscript and for helpful assistance; A. McIntosh from the Mathematical Sciences Institute at the Australian National University for discussions on the solution to the principal equations (7); and C. Jagadish from Electronic Materials Engineering for license access to CST MWS. This work has been partially supported by the Australian Research Council and the Australian Solar Institute.

- ¹M. Agio, *Nanoscale* **4**, 692 (2012).
- ²J.-J. Greffet, M. Laroche, and F. Marquier, *Phys. Rev. Lett.* **105**, 117701 (2010).
- ³A. Alu and N. Engheta, in *Proceedings of the Fourth European Conference on Antennas and Propagation (EuCAP)* (2010), pp. 1–3.
- ⁴E. M. Larsson, J. Alegret, M. Käll, and D. S. Sutherland, *Nano Lett.* **7**, 1256 (2007).
- ⁵H. A. Atwater and A. Polman, *Nature Mater.* **9**, 205 (2010).
- ⁶S. Mookapati, F. J. Beck, R. de Waele, A. Polman, and K. R. Catchpole, *J. Phys. D: Appl. Phys.* **44**, 185101 (2011).
- ⁷C. Balanis, *Antenna Theory: Analysis and Design*, 3rd ed. (Wiley-Interscience, 2005), Chap. 8, p. 433.
- ⁸A. Alu and N. Engheta, *Phys. Rev. Lett.* **101**, 043901 (2008).
- ⁹C. DeAngelis, D. A. Locatelli, D. Modotto, S. Boscolo, M. Midrio, F. Sacchetto, A. D. Capobianco, F. M. Pigozzo, and C. G. Someda, in *Proceedings of the 39th European Microwave Conference*, edited by EuMA (EuMA, Rome, Italy, 2009), pp. 810–813.
- ¹⁰A. Locatelli, C. D. Angelis, D. Modotto, S. Boscolo, F. Sacchetto, M. Midrio, A.-D. Capobianco, F. M. Pigozzo, and C. G. Someda, *Opt. Express* **17**, 16792 (2009).
- ¹¹G. W. Hanson, *IEEE Trans. Antennas Propag.* **54**, 3677 (2006).
- ¹²M. Staffaroni, J. Conway, S. Vedantam, J. Tang, and E. Yablonovitch, *Photonics Nanostruct. Fundam. Appl.* **10**, 166 (2012).
- ¹³V. Delgado, O. Sydoruk, E. Tatartschuk, R. Marqués, M. J. Freire, and L. Jelinek, *Metamaterials* **3**, 57 (2009).
- ¹⁴T. D. Corrigan, P. W. Kolb, A. B. Sushkov, H. D. Drew, D. C. Schmadel, and R. J. Phaneuf, *Opt. Express* **16**, 19850 (2008).
- ¹⁵F. Hao, E. M. Larsson, T. A. Ali, D. S. Sutherland, and P. Nordlander, *Chem. Phys. Lett.* **458**, 262 (2008).
- ¹⁶D. Ö. Güney, T. Koschny, and C. M. Soukoulis, *Phys. Rev. B* **80**, 125129 (2009).
- ¹⁷A. W. Clark and J. M. Cooper, *Small* **7**, 119 (2011).
- ¹⁸A. Locatelli, *IEEE Photon. J.* **3**, 845 (2011).
- ¹⁹D. R. Chowdhury, R. Singh, M. Reiten, J. Zhou, A. J. Taylor, and J. F. O'Hara, *Opt. Express* **19**, 10679 (2011).
- ²⁰O. Sydoruk, E. Tatartschuk, E. Shamonina, and L. Solymar, *J. Appl. Phys.* **105**, 014903 (2009).
- ²¹C. M. Dutta, T. A. Ali, D. W. Brandl, T.-H. Park, and P. Nordlander, *J. Chem. Phys.* **129**, 084706 (2008).
- ²²C. M. Soukoulis, T. Koschny, J. Zhou, M. Kafesaki, and E. N. Economou, *Phys. Status Solidi B* **244**, 1181 (2007).
- ²³J. Zhou, T. Koschny, M. Kafesaki, E. N. Economou, J. B. Pendry, and C. M. Soukoulis, *Phys. Rev. Lett.* **95**, 223902 (2005).
- ²⁴M. W. Klein, C. Enkrich, M. Wegener, C. M. Soukoulis, and S. Linden, *Opt. Lett.* **31**, 1259 (2006).
- ²⁵S. Tretyakov, *Metamaterials* **1**, 40 (2007).
- ²⁶T. Okamoto, T. Otsuka, S. Sato, T. Fukuta, and M. Haraguchi, *Opt. Express* **20**, 24059 (2012).
- ²⁷E. Tatartschuk, N. Gneiding, F. Hesmer, A. Radkovskaya, and E. Shamonina, *J. Appl. Phys.* **111**, 094904 (2012).
- ²⁸Y. Cai, Y. Li, P. Nordlander, and P. S. Cremer, *Nano Lett.* **12**, 4881 (2012).
- ²⁹A. R. Halpern and R. M. Corn, *ACS Nano* **7**, 1755 (2013).
- ³⁰A. F. McKinley, T. P. White, I. S. Maksymov, and K. R. Catchpole, *J. Appl. Phys.* **112**, 094911 (2012).
- ³¹J. E. Storer, "Impedance of the thin wire loop," *Technical Report* (Cruft Laboratory, Harvard University, 1955).
- ³²T. T. Wu, *J. Math. Phys.* **3**, 1301 (1962).
- ³³R. W. P. King, "The loop antenna for transmission and reception," in *Antenna Theory, Part 1*, 1st ed., Inter-University Electronic Series, Vol. 7, edited by R. E. Collin and F. J. Zucker (McGraw-Hill, New York, 1969), Chap. 11, pp. 458–482.
- ³⁴R. W. P. King, *The Theory of Linear Antennas* (Harvard University Press, Cambridge, MA, 1956).
- ³⁵R. King and T. Wu, *IEEE Trans. Antennas Propag.* **14**, 524 (1966).
- ³⁶J. Richmond, *IEEE Trans. Antennas Propag.* **15**, 802 (1967).
- ³⁷J. A. Stratton, *Electromagnetic Theory* (McGraw-Hill Book Company, New York and London, 1941).
- ³⁸L. Novotny, *Phys. Rev. Lett.* **98**, 266802 (2007).
- ³⁹P. B. Johnson and R. W. Christy, *Phys. Rev. B* **6**, 4370 (1972).
- ⁴⁰P. G. Etchegoin, E. C. L. Ru, and M. Meyer, *J. Chem. Phys.* **125**, 164705 (2006).
- ⁴¹P. G. Etchegoin, E. C. L. Ru, and M. Meyer, *J. Chem. Phys.* **127**, 189901 (2007).
- ⁴²A. Vial and T. Laroche, *J. Phys. D: Appl. Phys.* **40**, 7152–7158 (2007).
- ⁴³I. Stegun and M. Abramowitz, *Handbook of Mathematical Functions with Formulas, Graphs and Mathematical Tables, Applied Mathematics Series*, Vol. 55 (U.S. Government Printing Office, WDC, 1964), p. 1046.
- ⁴⁴See www.cst.com for Computer Simulation Technology AG, Microwave Studio, Darmstadt, Germany, 2012.
- ⁴⁵J. B. Khurgin and G. Sun, *Appl. Phys. Lett.* **99**, 211106 (2011).
- ⁴⁶G. Hanson, *IEEE Trans. Antennas Propag.* **50**, 66 (2008).
- ⁴⁷P. Schaffner, "Plasmonic excitations in nanometric gold ring structures with broken symmetry," Diplomarbeit (Master's) (Institut für Physik, Fachbereich Experimentalphysik, University of Graz, Graz, Austria, 2010).
- ⁴⁸C. Rockstuhl, T. Zentgraf, H. Guo, N. Liu, C. Etrich, I. Loa, K. Syassen, J. Kuhl, F. Lederer, and H. Giessen, *Appl. Phys. B: Lasers Opt.* **84**, 219 (2006).